Inorganic Chemistry

Article

pubs.acs.org/IC

Double Level Selection in a Constitutional Dynamic Library of Coordination Driven Supramolecular Polygons

Marzio Rancan,*[,†,‡] Jacopo Tessarolo,[†,‡] Maurizio Casarin,[†] Pier Luigi Zanonato,[†] Silvio Quici,[§] and Lidia Armelao[†,‡]

[†]Department of Chemical Sciences and INSTM, University of Padova, via Marzolo 1, 35131 Padova, Italy

[‡]IENI−CNR, via Marzolo 1, 35131 Padova, Italy

[§]ISTM−CNR, via C. Golgi, 19, 20133, Milano, Italy

Supporting Information

ABSTRACT: A constitutional dynamic library (CDL) of Cu(II) metallo-supramolecular polygons has been studied as a bench test to examine an interesting selection case based on molecular recognition. Sorting of the CDL polygons is achieved through a proper guest that is hosted into the triangular metallo-macrocycle constituent. Two selection mechanisms are observed, a guest induced path and a guest templated self-assembly (virtual library approach). Remarkably, the triangular host can accommodate several guests with a degree of selectivity ranging from ∼1 to ∼10^4 for all possible guest pairs. A double level selection operates: guests drive the CDL toward the triangular polygon, and, at the same time, this is able to pick a specific guest from a set of competitive molecules, according to a selectivity−affinity correlation. Association constants of the host−guest systems have been determined. Guest competition and exchange studies have been analyzed through variable temperature UV−Vis absorption spectroscopy and single crystal X-ray diffraction studies. Molecular structures and electronic properties of the triangular polygon and of the host−guest systems also have been studied by means of all electrons density functional theory (DFT) and time-dependent density functional theory (TDDFT) calculations including dispersive contributions. DFT outcomes ultimately indicate the dispersive nature of the host−guest interactions, while TDDFT results allow a thorough assignment of the host and host−guests spectral features.

INTRODUCTION

Self-assembly, organization, and selection processes of dynamic systems are particularly challenging since they represent a key step to obtain functional supramolecular objects toward complex matter.[1] Studies on metallo-supramolecular boxes and capsules have received increasing attention in the last two decades.[2] The self-assembly of these discrete architectures often generates more than one thermodynamically accessible structure in dynamic equilibrium.[3−5] Probably, the most reported case is the formation of triangular and square molecular polygons or boxes.[3a−j] Generally, such metallo-supramolecular dynamic systems can adapt their constitution in response to parameters such as concentration, solvent, and temperature[3a−k] or to external stimuli, such as guest-templating molecules (often anions).[3m−s,5] According to the concepts of constitutional dynamic chemistry (CDC),[6a] such systems can be described as examples of coordination driven constitutional dynamic libraries (CDLs),[6b] where more species are in equilibrium through continuous dissociation and recombination between metal ions and ligands. Hence, the capability to drive the system by controlling the equilibrating species through selection mechanisms becomes fundamental. The most powerful selection mechanisms in dynamic libraries are based on molecular recognition concepts. The selection can be ruled either by a thermodynamic or a kinetic control. A dynamic system is self-assembled starting from its initial building blocks, and the interchanging constituents can be subsequently selected by a chemical effector that specifically interacts with one of the library constituents. Alternatively, the library generation may be bypassed by adding the chemical effector to the initial building blocks. This latter approach illustrates the notion of virtual library (VL);[7] i.e., different constituents are virtually accessible, but only one is expressed via a molecular recognition mechanism.

In this context, we have employed a coordination CDL as a well tailored bench test to study the adaptation and selection processes taking place in a dynamic system driven by the molecular recognition of a target. Recently, some of us have reported the self-assembly of Cu^{2+} and ortho bis-(3-acetylacetone)benzene ligand (hereafter, *o*-LH_2) leading to a CDL of coordination polygons where a dimeric rhomboid ([Cu(*o*-L)]$_2$, hereafter {Cu_2}), and a trimeric triangle ([Cu(*o*-L)]$_3$, hereafter {Cu_3}), are both accessible.[4] Herein, we show

Received: March 13, 2014
Published: July 8, 2014

   dx.doi.org/10.1021/ic500573e | *Inorg. Chem.* 2014, 53, 7276−7287

that selection between the equilibrating species may be effectively operated through two different routes: (i) once the CDL constituents are assembled, the guest (G) induces the trimeric species selection leading to a host–guest triangle {G@Cu_3}; (ii) the same species is isolated starting from the building blocks (Cu^{2+}, *o*-LH_2, G) by a guest templated one-pot synthesis, according to the VL approach. A schematic representation of the two paths is displayed in Figure 1. A

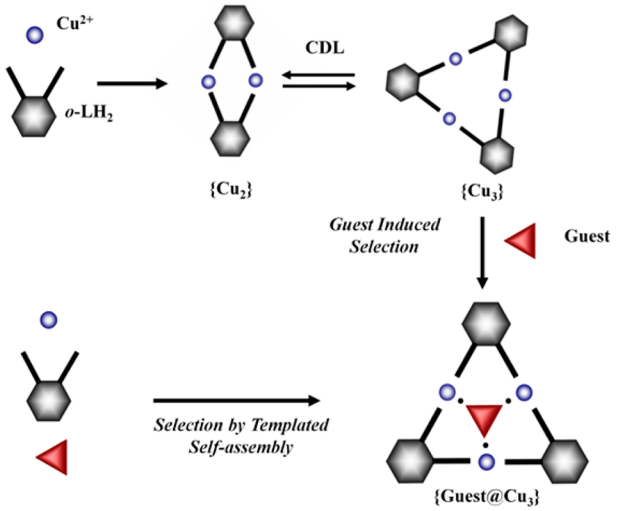

Figure 1. Representation of the two possible *molecular recognition* selection processes.

family of guest molecules with different shapes and coordination behaviors has been examined. Competition studies among the different guests ultimately proved the high degree of selection for the considered system, since only one molecular architecture is expressed over all possible combinations. {G@Cu_3} species easily undergo guest exchange. We also demonstrate that the selection is thermodynamically driven, as proven by the determined association constants for the host–guest triangles. A clear selectivity–affinity correlation is established among the different guests. To this regard, it is worthwhile to mention that such a thermodynamic selection, based on the molecular recognition mechanism, is reminiscent of the enzymatic lock and key model. A double level selection is established where guests act as CDL effectors toward the triangular metallo-supramolecular polygon, which, at the same time, is able to pick a specific guest from a set of competitive molecules.

The nature of these multifaceted systems has been unraveled by a combination of variable temperature UV–Vis absorption spectroscopy and single crystal X-ray diffraction studies. Further insights have been obtained by combining the experimental results with the outcomes of DFT–D3 quantum mechanical calculations.

RESULTS AND DISCUSSION

Cu^{2+} ions and *o*-LH_2 generate, by reversible assembly, a collection of coordination polygons.[4] Two species, a rhomboidal dimer and a triangular trimer, establish a dynamic equilibrium. Recently we showed that a phase change may be used to quantitatively select the rhomboidal polygon through crystallization.[4] On the other hand, in a preliminary work, it was also demonstrated that the trimeric species is sorted out through a suitable guest.[5] The selection relies on the possibility for the square planar Cu^{2+} ions to expand their coordination number by binding a proper target. Hence, the system re-equilibrates amplifying the species with the higher target affinity. The {Cu_3} molecular polygon is a trivalent host, since it has up to three possible binding sites with a local D_{3h} symmetry. Moreover, it is preorganized in a metallo-macrocycle with a triangular cavity. According to the complementarity concept,[8] host and guest have to fit not only in shape and size, but also chemically. Guest candidates need peculiar electronic and structural features such as the presence of σ-donor atoms, as well as the shape and size to fit the {Cu_3} cavity. A 3-fold symmetry is not mandatory, but it is a desirable trait to better interact with the triangular host. Six molecules have been chosen as possible guests (Chart 1): hexamethylenetetramine

Chart 1. Guest Candidates

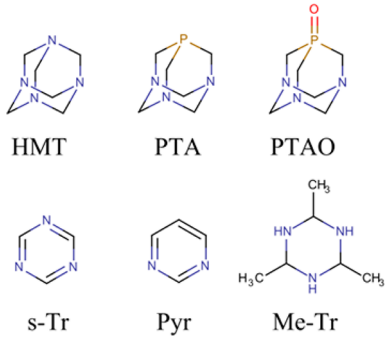

(HMT), 1,3,5-triaza-7-phosphaadamantane (PTA), 1,3,5-triaza-7-phosphaadamantane-7-oxide (PTAO), s-triazine (s-Tr), pyrimidine (Pyr), and 2,4,6-trimethyl-1,3,5-triazinane (Me-Tr). HMT has T_d symmetry, PTA, PTAO, s-Tr, and Me-Tr belong to the C_{3v} point group, and Pyr has C_{2v} symmetry. All of them are possible multivalent guests with nitrogen σ lone pairs. HMT is tetravalent, PTA, PTAO, s-Tr, and Me-Tr are trivalent, while Pyr is divalent. Elementary consideration allow us to foresee that aromatic and adamantane-like molecules should be characterized by some structural rigidity, while Me–Tr should be more flexible.

Guest Induced Selection. A guest solution has been added to a solution of {Cu_n} (n = 2, 3) CDL, prepared by dissolving dimer single crystals or the as obtained CDL powder[4] (molar ratio 3 Cu^{2+}/1 G). The solution instantly turns from olive green to blue-greenish, indicating a variation of the Cu^{2+} ions coordination. A similar behavior has been observed for all guests but one, i.e., Me–Tr.

The host–guest formation can be easily observed by absorption spectroscopy since it induces significant changes in the visible region (Figure 2). For HMT, s-Tr, PTA, and PTAO guests, all of them characterized by the presence of at least one 3-fold axis, the CDL band centered at 525 nm fades and two overlapped bands arise, centered around 620 and 730 nm. Such a behavior is not observed in the {Pyr@Cu_3} absorption spectrum. Here, the CDL band centered at 525 nm significantly decreases its relative intensity until becoming a shoulder of the band at 650 nm ca. As proven by X-ray diffraction measurements, in all cases but one, Cu^{2+} ions modify their coordinative environment moving from the square planar coordination in the CDL constituents to the square pyramidal one in the host–guest species. Guest molecules then act as chemical effectors for the quantitative selection of the trimer as a host–guest triangle, thus triggering a sorting of the system via

dx.doi.org/10.1021/ic500573e | Inorg. Chem. 2014, 53, 7276–7287

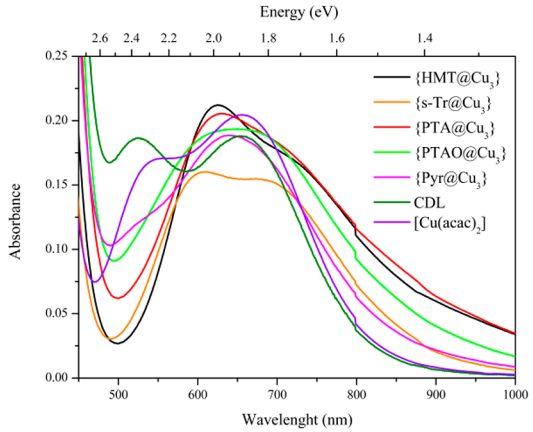

Figure 2. Absorption spectra of the CDL and $\{G@Cu_3\}$ species. The spectrum of $[Cu(acac)_2]$ has been also included for comparison.

a thermodynamic selection. The guest induced stimulus forces the CDL system to adapt itself to such a perturbation by shifting the equilibrium toward the triangle, as depicted in Figure 3.

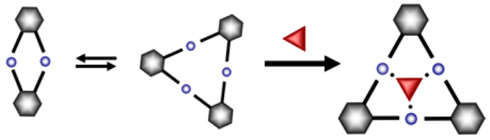

Figure 3. Guest molecule acts as an external stimulus for the guest induced selection of the CDL constituents.

Among the guests determining the instantaneous variations of the Cu^{2+} ions coordination, the only tested molecule missing a 3-fold symmetry is Pyr; nevertheless, it plays as an effective guest. This is probably due to host preorganization and to the mutual complementarity between $\{Cu_3\}$ and the Pyr guest, thus favoring the lock and key mechanism which rules the host–guest supramolecule formation. Two binding sites are enough to effectively interact with the triangle and stabilize it. At variance with all the other guests, Me–Tr does not induce any change in the CDL UV–Vis spectrum, thus suggesting that Me–Tr does not interact with $\{Cu_2\}$ nor $\{Cu_3\}$. The ineffectiveness of Me–Tr can be surely traced back to its inability, despite the presence of σ-donor atoms, to fit the triangular cavity. As a matter of fact, three floating methyl groups characterize the structure of the Me–Tr molecule, whose flexibility is certainly higher than that of the other guests. In the chair conformation, the methyl groups can flip from equatorial to axial positions leading to different conformers. The methyl groups are in the equatorial position, the most stable, and the inclusion in the preformed host cavity is not allowed due to steric hindrance.

Selection by Templated Self-Assembly. Once we demonstrated the possibility of managing a designed selection of a specific CDL constituent through a chemical effector, we explored how to bypass the CDL and obtain the supramolecular triangle in a one-pot synthesis. Such an approach implies that even if different constituents are virtually accessible, thus generating a VL, only one is expressed via a molecular recognition mechanism. The same guest molecule contemporary acts as the template and drives the host–guest triangle spawning via a self-assembly process (Figure 4).

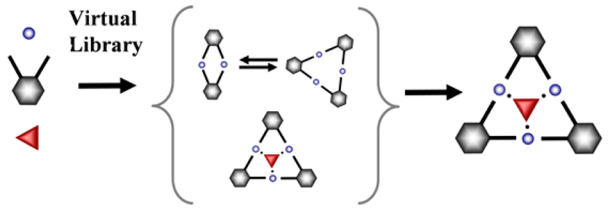

Figure 4. Templated self-assembly one-pot synthesis for the host–guest triangle. The system can be described as a virtual library.

The self-assembly one-pot synthesis has been carried out by exploiting a two-phase approach. The *o*-LH_2 ligand and the templating guest have been dissolved in the organic phase, while Cu^{2+} ions have been dissolved in the aqueous phase. Aqueous solutions of $[Cu(NH_3)_4]^{2+}$ or $Cu(OAc)_2{\cdot}H_2O$ have been used as sources for Cu^{2+} ions. The aqueous solution has been added to the organic one, and the system was left under vigorous stirring for 3 h. The organic phase color turned instantaneously from pale yellow to the blue-greenish, as previously observed in the guest induced selection. UV–Vis absorption analysis yielded exactly the same spectra reported in Figure 2. The two phases have been then separated, and the organic one has been evaporated under reduced pressure affording the desired product. The compounds identity has been also confirmed by single crystal X-ray studies. As expected, a similar behavior has been observed for all guests with the exception of Me–Tr.

Structural Studies. The new host–guest compounds have been isolated as single crystals in quantitative or high yield (>70%). X-ray diffraction studies confirm the host–guest structure of the $\{G@Cu_3\}$ species. $\{HMT@Cu_3\}$, $\{s\text{-}Tr@Cu_3\}$, and $\{PTAO@Cu_3\}$ can be crystallized from various solvent mixtures; selected examples are here reported. Figures 5–9

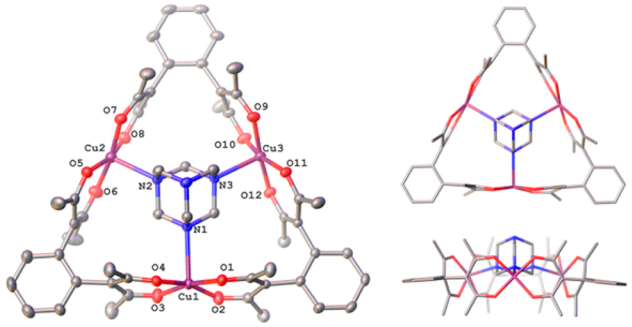

Figure 5. Structure of $\{HMT@Cu_3\}$ from chloroform/ethanol. Selected bond distances (Å): Cu1–O1 1.936(3), Cu1–O2 1.919(3), Cu1–O3 1.909(3), Cu1–O4 1.929(3), Cu1–N1 2.421(3), Cu2–O5 1.936(3), Cu2–O6 1.915(3), Cu2–O7 1.926(3), Cu2–O8 1.928(3), Cu2–N2 2.364(3), Cu3–O9 1.926(3), Cu3–O10 1.906(3), Cu3–O11 1.930(3), Cu3–O12 1.917(2), Cu3–N3 2.364(3). Top and side views (capped stick models). Thermal ellipsoids drawn at the 30% probability level. H atoms omitted for clarity.

display compounds structures along with selected bond lengths for Cu^{2+} ions coordination sphere. Complete crystallographic data and details of data collections are reported in the Supporting Information for all obtained single crystals. All Cu^{2+} ions, except one in $\{Pyr@Cu_3\}$, have a similar distorted square pyramidal coordination with four acetylacetonate oxygen atoms at the equatorial plane and a guest nitrogen atom in the apical position. The $Cu–O_{acac}$ and the $Cu–N_{guest}$

dx.doi.org/10.1021/ic500573e | Inorg. Chem. 2014, 53, 7276–7287

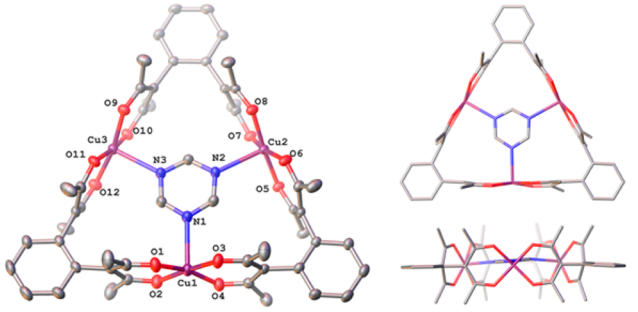

Figure 6. Structure of {s-Tr@Cu_3} from chloroform/*n*-hexane. Selected bond distances (Å): Cu1−O1 1.923(4), Cu1−O2 1.916(4), Cu1−O3 1.923(4), Cu1−O4 1.906(4), Cu1−N1 2.368(5), Cu2−O5 1.914(4), Cu2−O6 1.917(4), Cu2−O7 1.928(4), Cu2−O8 1.919(4), Cu2−N2 2.374(4), Cu3−O9 1.924(4), Cu3−O10 1.914(4), Cu3−O11 1.926(4), Cu3−O12 1.917(4), Cu3−N3 2.384(5). Top and side views (capped stick models). Thermal ellipsoids drawn at the 30% probability level. H atoms and solvent molecules omitted for clarity.

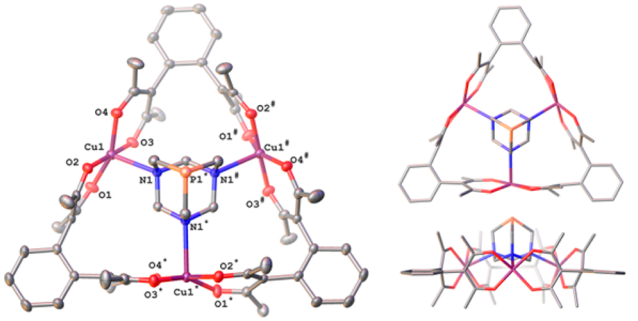

Figure 7. Structure of {PTA@Cu_3} from chloroform/cyclohexane. Selected bond distances (Å): Cu1−O1 1.927(3), Cu1−O2 1.923(3), Cu1−O3 1.908(3), Cu1−O4 1.938(3), Cu1−N1 2.437(3). Symmetry operations: *1 − *y*, 1 + *x* − *y*, +*z* and #*y* −*x*, 1 − *x*, +*z*. Top and side views (capped stick models). Thermal ellipsoids drawn at the 30% probability level. H atoms and solvent molecules omitted for clarity.

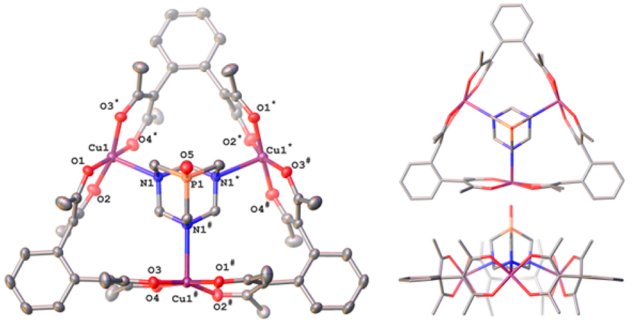

Figure 8. Structure of {PTAO@Cu_3} from chloroform/toluene. Selected bond distances (Å): Cu1−O1 1.934(3), Cu1−O2 1.908(3), Cu1−O3* 1.931(3), Cu1−O4* 1.911(3), Cu1−N1 2.474(3), P1−O5 1.486(5). Symmetry operations: *1+*y* − *x*, 1 − *x*, +*z* and #1 −*y*, *x* − *y*, +*z*. Top and side views (capped stick models). Thermal ellipsoids drawn at the 30% probability level. H atoms and solvent molecules omitted for clarity.

internuclear distances span the intervals 1.906−1.938 Å and 2.316−2.474 Å, respectively. In {Pyr@Cu_3}, one copper atom (Cu3 in Figure 9) has a distorted square planar coordination. In this case, the Cu−O_{acac} lengths are sligthly shorter (1.877−1.902 Å). Pyrimidine has two nitrogen σ-donor atoms (N1 and N2); hence, only two Cu^{2+} ions are involved in the host−guest

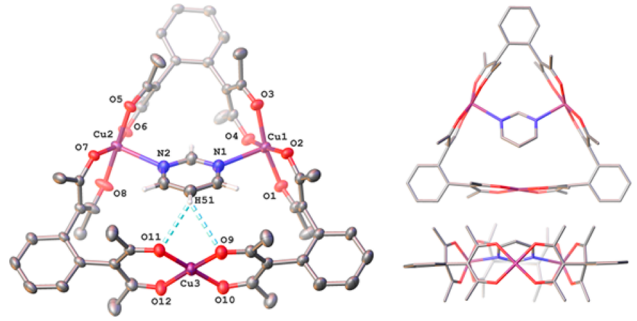

Figure 9. Structure of {Pyr@Cu_3} from chloroform/decane. Selected bond distances (Å): Cu1−O1 1.920(4), Cu1−O2 1.924(4), Cu1−O3 1.928(4), Cu1−O4 1.928(4), Cu1−N1 2.316(5),Cu2−O5 1.921(4), Cu2−O6 1.923(4), Cu2−O7 1.935(4), Cu2−O8 1.907(4), Cu2−N2 2.340(5), Cu3−O9 1.902(4), Cu3−O10 1.894(4), Cu3−O11 1.903(4), Cu3−O12 1.877(4), O11···H51 2.462(4), O9···H51 2.567(5). Top and side views (capped stick models). Thermal ellipsoids drawn at the 30% probability level. H atoms and solvent molecules omitted for clarity.

interaction; nevertheless, as already mentioned, this is enough to retain the triangular shape and to stabilize it. When dealing with guests having a 3-fold symmetry, Cu···Cu internuclear distances and Cu···Cu···Cu angles are in the intervals 6.3−6.5 Å and 59°−62°, respectively. At variance to that, the absence of any C_3 axis in the pyrimidine molecule induces larger distorsions in the {Pyr@Cu_3} geometrical parameters when compared to the other {G@Cu_3} (internuclear distances between penta- and tetracoordinated Cu^{2+} ions—Cu1···Cu3 and Cu2···Cu3—are in the interval 6.6−6.7 Å, while the Cu1···Cu3···Cu2 angle is 57°).

A comparison among the host−guest architectures shows that guests enter the triangle cavity interacting with Cu^{2+} ions, as designed. The most significant structural difference lies in the occupation of the triangle cavity (Table 1 and Figure 10). s-

Table 1. Cu^{2+} Ions Mean Plane σ_{Cu}···N Distances (Å)

	σ_{Cu}···N1	σ_{Cu}···N2	σ_{Cu}···N3	$(\sigma_{Cu}$···N$)_{theory}$
Cu_3@HTM	0.619	0.610	0.628	0.638
Cu_3@PTA	0.951	0.951	0.951	0.912
Cu_3@PTAO	0.911	0.911	0.911	0.923
Cu_3@s-Tr	0.082	0.100	−0.185	0.000
Cu_3@Pyr	0.355	0.404		0.447

Triazine perfectly fits the host cavity and becomes almost coplanar with the plane defined by the three Cu^{2+} ions (σ_{Cu}). At variance to that, the slightly bulkier adamantane-like guests (HMT, PTA, and PTAO) are shifted out of σ_{Cu}. Finally, even if pyrimidine nitrogen atoms are quite close to σ_{Cu}, the lack of the third binding site induces a tilting of the guest molecule in the triangular cavity. The tilt angle between σ_{Cu} and the pyrimidine aromatic ring is ∼32°. As a consequence of this tilt, two nonclassical hydrogen bonds between a Pyr H atom and two acetylacetonate oxygen atoms (O11···H51 2.462 Å and O9···H51 2.567 Å, Figure 9) are present.

Optimized structural parameters of {G@Cu_3} complexes satisfactorily match X-ray data (G, {Cu_3}, and {G@Cu_3} Cartesian coordinates, optimized either by including or by neglecting dispersive contributions are collected in Tables S30−S41 of Supporting Information). In particular, they are able to capture: (i) the s-Tr perfect fit of the host cavity and its

dx.doi.org/10.1021/ic500573e | *Inorg. Chem.* 2014, 53, 7276−7287

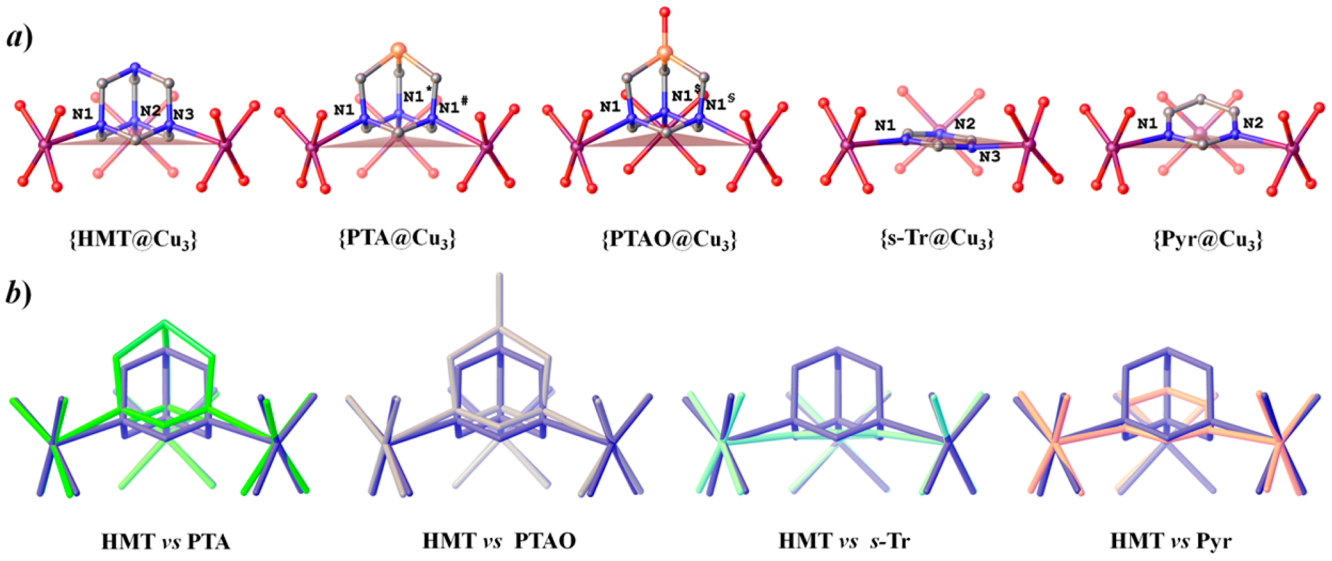

Figure 10. (a) $\{[CuO_4]_3G\}$ moieties and occupation of the triangle cavity. (b) Overlay of different $\{[CuO_4]_3G\}$ moieties: $\{[CuO_4]_3HMT\}$ has been chosen as basis for comparison along guests set. Symmetry operations: $^{*}1-y, 1+x-y, +z$, $^{\#}y-x, 1-x, +z$, $^{\$}1+y-x, 1-x, +z$ and $^{\S}1-y, x-y, +z$.

co-planarity with the σ_{Cu} plane; (ii) the HMT, PTA, and PTAO shift out of the σ_{Cu} plane; (iii) the tilting of the Pyr molecule in the triangular cavity. Incidentally, the optimized tilt angle between σ_{Cu} and the pyrimidine aromatic ring is ∼42°, i.e., significantly larger than that experimentally found (∼32°). Most probably, such a result may be traced back to the flatness of the corresponding potential energy surface. A further point deserving some comment concerns the optimized structure of the $\{Cu_3\}$ free host (Figure 11) for which single crystals cannot

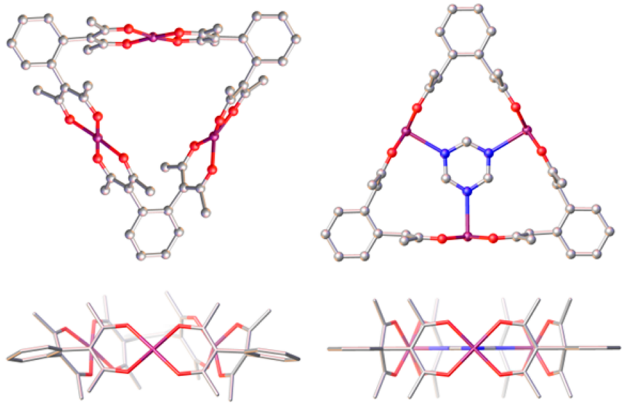

Figure 11. Otpmized structures of the $\{Cu_3\}$ host and the $\{s\text{-}Tr@Cu_3\}$ supramolecule. Top view (top) and lateral view (bottom).

be obtained. The inspection of Figure 11 ultimately testifies the essential role played by the guests in determining the $\{G@Cu_3\}$ high local symmetry. This suggests that, to effectively host the guests, $\{Cu_3\}$ needs to rearrange with a significant energy cost (ΔE_{prep}^{host}) despite its preorganization in a triangular macrocycle. In particular, host preparation energies (Table 4) are significantly higher for the adamantane-like guests compared to the aromatic ones. Finally, guests preparation energies (ΔE_{prep}^{guest}) are negligible due to their structural rigidity.

Guests Competition Studies. Competition studies among the different guest molecules (HMT, s-Tr, PTA, PTAO, and Pyr) have been performed to compare their behavior, simultaneously increasing the system complexity. Both routes discussed above have been explored. In the guest induced selection path, a solution containing equimolar amounts of the five guests has been added to a CDL solution (molar ratio 3 Cu^{2+}/1 Gs), Figure 12. The solution instantly turned from olive

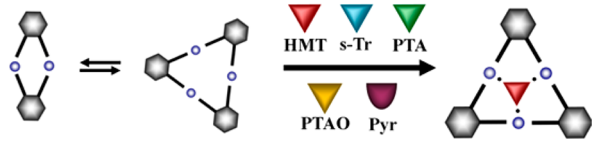

Figure 12. Competition studies among the different guests starting from the CDL system.

green to blue-greenish, and it was left under stirring for few hours and then evaporated. UV−Vis absorption spectra suggested the formation of the $\{HMT@Cu_3\}$ host−guest species. After crystallization (quantitative), single crystal X-ray diffraction ultimately confirmed the nature of the product.

Competition studies among the different guests and the CDL show that a double level selection is established. Guests are able to selectively bind the triangular constituent, which, at the same time, is able to pick a specific guest from a set of competitive molecules. In the templated self-assembly route, a VL has been generated by combining the five guests, the *o*-LH_2 ligand and Cu^{2+} ions (Figure 13). An aqueous solutions of Cu^{2+} ions has been added to an organic phase containing the ligand and the guests (molar ratio 3 Cu^{2+}/3 *o*-LH_2/1 Gs). The mixture has been then stirred for 2 h, although the organic phase instantaneously changed its color turning from pale yellow to blue-greenish. The obtained product has been characterized by UV−Vis absorption spectroscopy and once again identified as $\{HMT@Cu_3\}$. Moreover, single crystals of the host−guest triangle containing HMT have been obtained (quantitative yield). Single crystal X-ray diffraction has been used to further confirm the product identity.

Guests Exchange Studies. Competition studies have demonstrated that the formation of $\{HMT@Cu_3\}$ is favored over all the other investigated host−guest species. To access if a

dx.doi.org/10.1021/ic500573e | Inorg. Chem. 2014, 53, 7276−7287

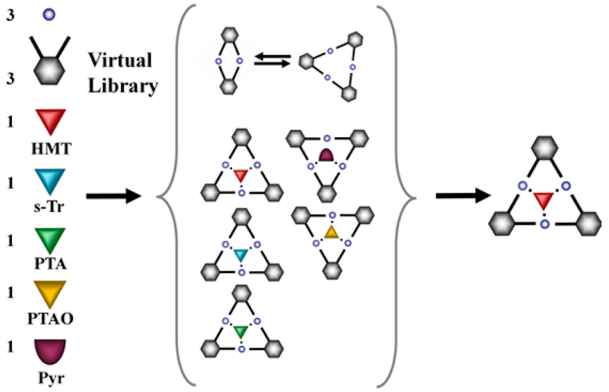

Figure 13. Competition studies among the different guests through the VL system.

guest can displace another guest already accommodated into the triangular cavity, single crystals of $\{G@Cu_3\}$ have been dissolved in chloroform, and a guest competitor, G', has been added in an equimolar amount. As soon as the exchange took place, a color variation was observed within a few minutes; this was confirmed by UV–Vis spectroscopy by comparison with the spectrum of the $\{G'@Cu_3\}$ solution. First, HMT has been tested as competitor. It can easily replace all the other guests in the $\{G@Cu_3\}$ assemblies (G = s-Tr, PTA, PTAO, and Pyr). Conversely, none of the guests can replace HMT in the triangle pocket. s-Tr can replace PTA, PTAO, and Pyr, and can be replaced only by HMT. PTA and PTAO can replace only Pyr. Interestingly, when the exchange reaction is performed between PTA and PTAO, the corresponding absorption spectra indicate that both $\{PTA@Cu_3\}$ and $\{PTAO@Cu_3\}$ are present in equilibrium in solution. On the basis of these observations, the following empirical scale for the host–guest affinity can be deduced: HMT > s-Tr > PTA ≈ PTAO > Pyr.

Host–Guest Equilibrium Studies. To better investigate the thermodynamic aspects of the selection process, the host–guest association constants have been determined at variable temperature. For non-paramagnetic metal species this is usually done by NMR, but due to the presence of Cu^{2+} ions useful NMR data cannot be obtained. On the other hand, in this case UV–Vis absorption spectroscopy is a suitable method to study the formation of the host–guest triangle due to the color change that occurs during the process. Since the trimer concentration is governed by the CDL eq 1, it was included in the speciation model. Equation 1 has been previously[4] investigated, and a value of log K_{DT} = 4.8 was determined.

$$3\{Cu_2\} \rightleftharpoons 2\{Cu_3\}\ (K_{DT}) \quad (1)$$

$$\{Cu_3\} + G \rightleftharpoons \{G@Cu_3\}\ (K_{as}) \quad (2)$$

The guest has been added batchwise to a CDL solution at constant temperature, and absorption spectra have been collected. Successively, data analysis has been performed according to the model described in Supporting Information. Figure 14 shows the results of the titration with s-Tr at 293.15 and 308.15 K. The results for the other guests and temperatures are reported in Supporting Information (Figures S8–S28). Upon addition of the guest, spectra change significantly: the main difference is the progressive disappearance of the CDL band centered at 525 nm. Two overlapped bands centered at 610 and 700 nm appear and an isosbestic point at 715 nm (293.15 K), and at 701 nm (308.15 K), is clearly visible. Figure

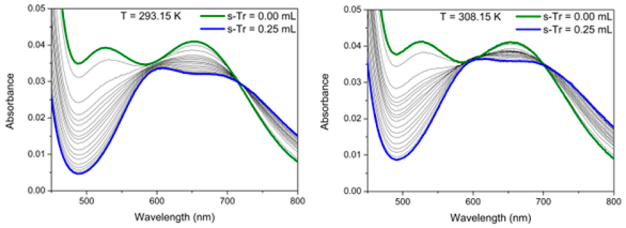

Figure 14. CDL titration with s-Tr at 293.15 and 308.15 K.

15a reports the experimental (293.15 K) and calculated absorption at 500 nm along with the speciation plot, while

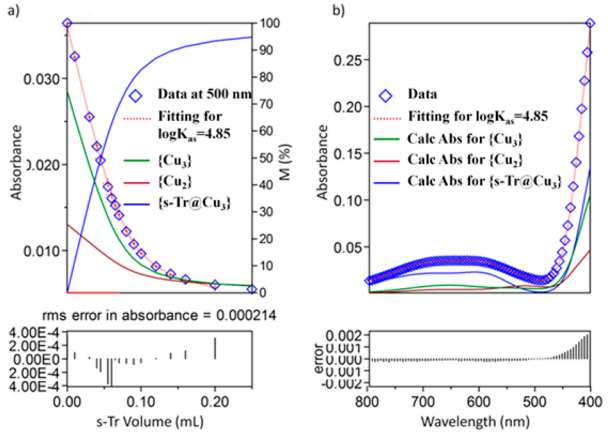

Figure 15. CDL titration with s-Tr. (a) Absorbance variation at 500 nm (293.15 K) and fitting for log K_{as} = 4.85; % fraction of $\{Cu_2\}$, $\{Cu_3\}$, and $\{s\text{-}Tr@Cu_3\}$ as a function of the total virtual monomer (M = [Cu(*o*-L)], Supporting Information) concentration. (b) Experimental and calculated absorption spectra after addition of 0.06 mL of a 11.80 mM s-Tr solution to a 0.96 mM CDL solution at 293.15 K.

Figure 15b shows a comparison between experimental and calculated spectra after the addition of s-Tr (0.06 mL).

Thermodynamic parameters are of interest to better understand the enthalpic and entropic contribution to the formation of the host–guest species. To this aim, titration spectra have been recorded at different temperatures in the interval ranging from 288.15 and 308.15 K. Calculated association constants are reported in Table 2. By means of

Table 2. Host–Guest Association Constants

T (K)	log K_{HMT}	log $K_{s\text{-}Tr}$	log K_{PTA}	log K_{PTAO}	log K_{Pyr}
288.15	6.68 (9)		3.49 (1)		
293.15	6.55 (3)	4.85 (1)	3.39 (1)	3.22 (1)	2.50 (1)
298.15	6.28 (3)	4.64 (1)	3.39 (2)	3.11 (1)	2.37 (1)
303.15	6.12 (4)	4.52 (3)	3.30 (2)	3.07 (2)	2.22 (2)
308.15		4.31 (2)	3.25 (1)	2.89 (1)	2.09 (2)

the van't Hoff equation, $\Delta H°$ and $\Delta S°$ have been determined (van't Hoff plots are reported in Supporting Information). As expected for association of neutral species, the formation of the host–guest supramolecule is exothermic, while unfavorable entropic terms show that changes of species solvation do not give a significant contribution to the overall stability. However, the entropic term is relevant to the selection process as it introduces important differences in the order of stability of the adducts. In fact, the order of the enthalpies of formation is $\Delta H°_{HMT} > \Delta H°_{s\text{-}Tr} > \Delta H°_{Pyr} > \Delta H°_{PTAO} > \Delta H°_{PTA}$, while the

dx.doi.org/10.1021/ic500573e | Inorg. Chem. 2014, 53, 7276–7287

Table 3. Thermodynamic Parameters for the Host−Guest Association at 298.15 K

	HMT	s-Tr	PTA	PTAO	Pyr
ΔH° (kJ mol^{-1})	−74.47 (±6.99)	−62.20 (±2.41)	−19.82 (±1.16)	−37.80 (±3.75)	−47.42 (±2.32)
ΔS° (J mol^{-1} K^{-1})	−129 (±23)	−120 (±8)	−2 (±4)	−67 (±13)	−114 (±8)
ΔG° (kJ mol^{-1})	−35.85 (±0.14)	−26.48 (±0.06)	−19.35 (±0.12)	−17.75 (±0.06)	−13.53 (±0.06)

Table 4. {G@Cu_3} BEs (kJ/mol, No Dispersion Corrected Values in Parentheses) Decomposed According to the Ziegler Transition-State Method

	BE	ΔE_{prep}^{guest}	ΔE_{prep}^{host}	BE_{corr}
{HMT@Cu_3}	−221.39 (−63.30)	0.33 (0.00)	54.71 (43.54)	−166.34 (−19.76)
{PTA@Cu_3}	−207.11 (−44.00)	3.06 (2.18)	64.25 (52.50)	−139.81 (10.68)
{PTAO@Cu_3}	−208.96 (−44.59)	2.34 (1.55)	60.07 (46.89)	−146.54 (3.85)
{s-Tr@Cu_3}	−134.87 (−46.47)	1.42 (0.17)	38.02 (22.65)	−95.43 (−23.64)
{Pyr@Cu_3}	−134.49 (−45.51)	1.55 (1.00)	24.49 (17.12)	−108.45 (−27.39)

free energies follow the order $\Delta G^\circ_{HMT} > \Delta G^\circ_{s\text{-}Tr} > \Delta G^\circ_{PTA} \approx \Delta G^\circ_{PTAO} > \Delta G^\circ_{Pyr}$. Also, this latter trend confirms the empirical scale for the host−guest affinity observed in the guest exchange studies.

Guest Selectivity. The thermodynamic selectivity ($S_{HG/HG'}$) of a host (H) toward two competitor guests (G, G') can be quantified as the ratio between their association constants as follows:[8,9]

$$S_{HG/HG'} = K_{HG}/K_{HG'} \quad (3)$$

Hence, from data reported in Table 2, the selectivity of the {Cu_3} host toward all the possible guest pairs is promptly derived (Table 5). These data explain well the results obtained by competition and guest exchange studies. {Cu_3} is ∼50-fold more selective toward HMT over s-Tr, and the selectivity increases by a factor of 10^2−10^3 when HMT competes with other guests. For instance, it rises up to 8.13×10^3 when considering the pair HMT/Pyr. Moreover, one can explain why the exchange reaction between PTA and PTAO (or vice versa) is not effective, being $S_{PTA/PTAO} = 2$.

Table 5. Host Selectivity toward Guest Pairs at 298.15 K

guest pair	S
HMT/Pyr	8130
HMT/PTAO	1480
HMT/PTA	776
s-Tr/Pyr	186
HMT/s-Tr	44
s-Tr/PTAO	34
s-Tr/PTA	18
PTA/Pyr	11
PTAO/Pyr	6
PTA/PTAO	2

Theoretical Results. Besides information about the structures of isolated species, DFT calculations have been also useful to look into the nature of the host−guest interaction, as well as to rationalize the CDL and {G@Cu_3} UV−Vis spectroscopic data. As far as the former point is concerned, relative positions of adamantane-like guests in the energy scale (Table 3) are reproduced by {G@Cu_3} binding energies (BEs) values decomposed according to the Ziegler transition-state method.[10]

Moreover, theoretical data clearly indicate that (i) the host−guest interaction is mainly dispersive in nature; (ii) the bulkiest guests imply significant ΔE_{prep}^{host}; (iii) the inclusion of dispersive interactions is essential to achieve {PTA@Cu_3} and {PTAO@Cu_3} bound systems. Nevertheless, the comparison of data reported in Table 4 with those of Table 3 stresses that the *agreement* between ΔH° and {G@Cu_3} BEs is limited to the evidence that HMT corresponds to the most tightly bound guest. As a whole, association enthalpies are poorly reproduced by BE values. At variance to that, ADF calculations coupled to magnetic[11] and structural evidence are very useful to rationalize the CDL and {G@Cu_3} spectroscopic properties (Figure 2). Magnetic studies[11] pertinent to a dinuclear Cu^{2+} complex of the *o*-LH_2 ligand are in fact consistent with two independent Cu^{2+} ions. More specifically, the magnetic coupling mediated by the *o*-LH_2 ligand is negligible, and the magnetic orbital lies in the CuO_4 plane. Such evidence prompted us to assume an analogous behavior for the {Cu_3} Cu^{2+} ions.

As far as structural outcomes are concerned, X-ray diffraction data herein reported indicate that the coordination sphere of each Cu^{2+} ion is substantially the same of that characterizing the [$Cu(acac)_2$] (acac = acetylacetonate) species eventually perturbed by the presence of a fifth nitrogen based ligand. On these bases, theoretical and experimental results pertaining to [$Cu(acac)_2$] may be used as a guideline to assign the CDL and {G@Cu_3} UV−Vis absorption spectra.

Even though the electronic structure of [$Cu(acac)_2$] has been recently revisited by de Almeida et al. by means of spin-restricted open-shell DFT calculations,[12] we decided to carry out a further series of spin-unrestricted DFT numerical experiments on the D_{2h} [$Cu(acac)_2$] to compare theoretical results homogeneous between them.[13] In this regard, it is also worth noting that Wang and Ziegler have shown that spin-unrestricted time-dependent (TD) DFT calculations are able to provide rather accurate estimates of excitation energies (EEs) even for open shell molecules.[14]

The [$Cu(acac)_2$] ground state (GS) is characterized by the presence of a single hole in a Cu^{2+} 3d-based orbital (the $3d_{xy}$, in the adopted framework), thus resulting in a doublet state. EEs imply either transitions to this singly occupied MO or transitions to completely unoccupied MOs. In the former case, both GS and excited states correspond to doublet states, if spin contamination is neglected, while two doublet states and one quartet state are generated in the latter. Our interest is limited to formally forbidden d−d transitions, so that doublet → quartet transitions, implying spin−flip or double excitation processes, will be herein ignored, and [$Cu(acac)_2$] UV−Vis evidence will be tackled by only considering doublet → doublet excitations.

dx.doi.org/10.1021/ic500573e | Inorg. Chem. 2014, 53, 7276−7287

Now, before entering into the detail of ADF results, a qualitative picture of the metal−ligand bonding scheme, simply based on symmetry arguments, can be useful to better understand the forthcoming discussion. The square planar arrangement of the central Cu^{2+} ion in $[Cu(acac)_2]$ lifts the five-fold degeneracy of the Cu 3d atomic orbitals (AOs) to generate, in a perfect D_{4h} arrangement, four low-lying, completely occupied, MOs of symmetry a_{1g}, b_{1g}, and e_g as well as a single occupied b_{2g} level. Moreover, metal−ligand interactions involving Cu 3d based a_{1g} (z^2), b_{1g} ($x^2 - y^2$), and b_{2g} (xy) AOs will have a σ character, while those implying the e_g (xz, yz) orbitals will be π in nature. When the actual symmetry of the $[Cu(acac)_2]$ molecule (D_{2h}) is taken into account, the following correlations have to be considered: $a_{1g} \rightarrow a_g$, $b_{1g} \rightarrow a_g$, $e_g \rightarrow b_{2g} + b_{3g}$, $b_{2g} \rightarrow b_{1g}$. Spin up (↑) and spin down (↓) bonding/antibonding combinations of Cu 3d AOs and ligand based MOs of symmetry a_g, b_{2g}, and b_{3g} will be completely occupied. The same holds for bonding and antibonding partners of the $^{\uparrow}b_{1g}$ σ interaction, while the $^{\downarrow}b_{1g}$ antibonding combination is empty. These considerations allow us to rationalize data reported in Figure 16, where Cu 3d PDOS and Cu−O COOPs spin ↓ are displayed. The $11^{\downarrow}b_{1g}$ lowest unoccupied MO (LUMO), strongly localized on the Cu $3d_{xy}$ AO (64%), is the only $^{\downarrow}b_{1g}$ orbital having a Cu−O antibonding character (see the corresponding negative COOP in Figure 16). At variance to that, $^{\downarrow}a_g$ ($x^2 - y^2$, z^2), $^{\downarrow}b_{2g}$ (xz), and $^{\downarrow}b_{3g}$ (yz) Cu 3d based orbitals do not provide any contribution to the Cu−O bond, being corresponding bonding and antibonding combinations with suitable ligand based MOs completely occupied. Interestingly, the $4^{\downarrow}b_{3g}$ HOMO corresponds to a π-ligand based MO, Cu−O antibonding (Figure 17), with a minor localization (6%) on the Cu $3d_{yz}$ AO.

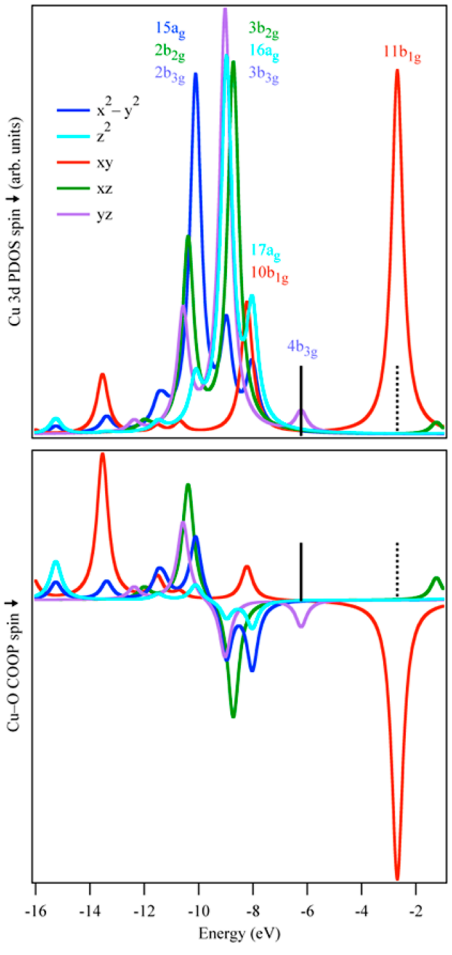

Figure 16. $[Cu(acac)_2]$ 3d spin ↓ PDOS and Cu−O spin ↓ COOPs. Positive (negative) COOP values correspond to bonding (antibonding) interactions. Vertical bars mark the HOMO (full line) and LUMO (dotted line) energies.

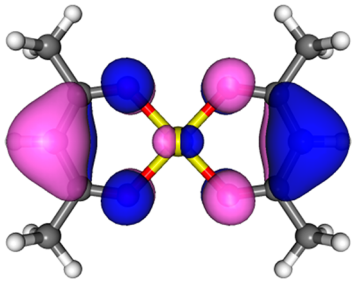

Figure 17. 3D contour plots of the $[Cu(acac)_2]$ $4^{\downarrow}b_{3g}$ HOMO. Pink (blue) surfaces correspond to the positive (negative) value of 0.05 (−0.05) $e^{1/2}$ $Å^{-3/2}$.

$[Cu(acac)_2]$ spin-unrestricted TDDFT doublet−doublet lowest lying EEs[14a] imply transitions to the $11^{\downarrow}b_{1g}$ LUMO; their symmetries, energies and compositions are b_{2g} (1.98 eV; $4^{\downarrow}b_{3g} \rightarrow 11^{\downarrow}b_{1g}$ (73%) + $3^{\downarrow}b_{3g} \rightarrow 11^{\downarrow}b_{1g}$ (25%)); b_{1g} (2.38 eV; $17^{\downarrow}a_g \rightarrow 11^{\downarrow}b_{1g}$ (70%) + $15^{\downarrow}a_g \rightarrow 11^{\downarrow}b_{1g}$ (25%)); b_{1g} (2.63 eV; $16^{\downarrow}a_g \rightarrow 11^{\downarrow}b_{1g}$ (86%) + $15^{\downarrow}a_g \rightarrow 11^{\downarrow}b_{1g}$ (11%)); b_{3g} (2.63 eV; $3^{\downarrow}b_{2g} \rightarrow 11^{\downarrow}b_{1g}$ (86%) + $2^{\downarrow}b_{3g} \rightarrow 11^{\downarrow}b_{1g}$ (13%)).[15]

The PDOS labeling of Figure 16 allows us to associate these four transitions to Cu^{2+} based, formally forbidden,[16] d−d excitations; nevertheless, the composition of the b_{2g} one clearly indicates the significant contribution of the HOMO → LUMO transition to the lowest lying excitation. The $[Cu(acac)_2]$ spectrum in the energy range extending from 490 nm (2.53 eV) to 800 nm (1.55 eV) is characterized by the presence of two overlapping bands centered at 653 and ∼550 nm (∼1.90 and ∼2.25 eV, respectively; Figure 2). The comparison of experimental evidence with TDDFT outcomes suggests assignment of the lowest lying EE to a transition mainly involving the $4^{\downarrow}b_{3g}$ HOMO → $11^{\downarrow}b_{1g}$ LUMO excitation, while transitions from Cu 3d-based $^{\downarrow}$MO to the $11^{\downarrow}b_{1g}$ LUMO would contribute to the feature centered at ∼2.25 eV. As a whole, $[Cu(acac)_2]$ spectroscopic data in the UV−Vis energy region are satisfactorily reproduced by spin-unrestricted TDDFT doublet−doublet calculations, thus confirming the validity of the adopted approach to investigate open shell systems.[14]

Moving to $\{Cu_3\}$, its electronic properties may be worked out by taking advantage of the presence of three independent Cu^{2+} ions having the same coordination sphere of copper in $[Cu(acac)_2]$. In particular, the absence of any *communication* among metal ions coupled to the presence of a local three-fold axis allows us to foresee some parenthood between $\{Cu_3\}$ HOMOs (LUMOs) and linear combinations of the $[Cu(acac)_2]$ $4^{\downarrow}b_{3g}$-like ($11^{\downarrow}b_{1g}$-like) level.

These preliminary considerations perfectly fit ADF results; in particular, the $\{Cu_3\}$ $^{\downarrow}$HOMOs ($^{\downarrow}$LUMOs) correspond to the three closely spaced $256^{\downarrow}a$−$258^{\downarrow}a$ ($259^{\downarrow}a$−$261^{\downarrow}a$) MOs having negligible (significant) localizations on Cu 3d AOs (Figure 18) and strongly reminiscent of the $[Cu(acac)_2]$ $4^{\downarrow}b3g$ HOMO ($11^{\downarrow}b_1g$ LUMO). Moreover, the $\{Cu_3\}$ 3d ↓ PDOS in the −8 to −10 eV energy range is dominated by two main peaks

dx.doi.org/10.1021/ic500573e | Inorg. Chem. 2014, 53, 7276−7287

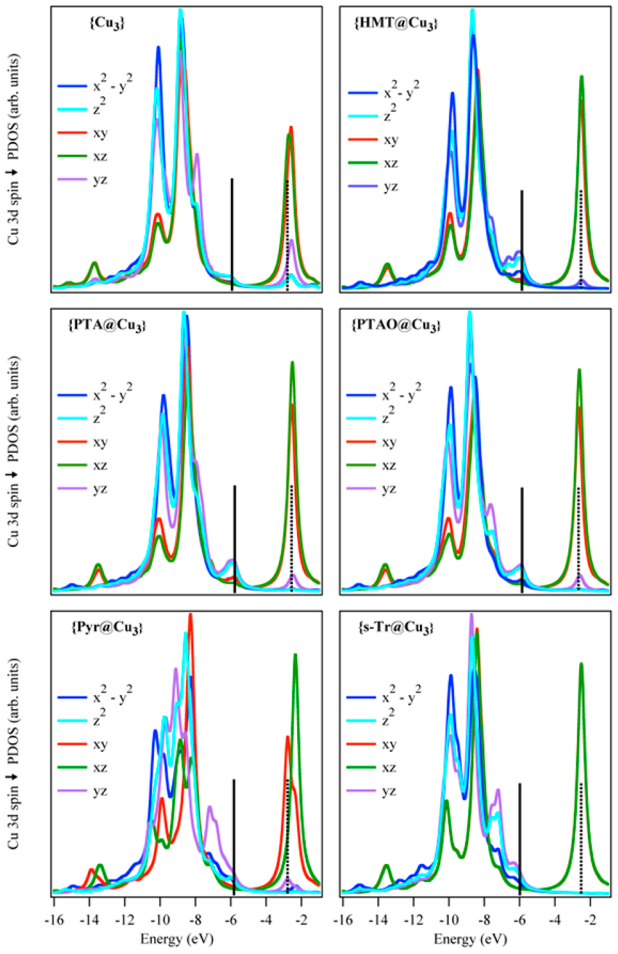

Figure 18. $\{Cu_3\}$ and $\{G@Cu_3\}$ 3d spin ↓ PDOS. Vertical bars mark the HOMO (full line) and LUMO (dotted line) energies.

corresponding to the linear combinations of the $[Cu(acac)_2]$ based $10^{\downarrow}b_{1g}$, $17^{\downarrow}a_g$, $3^{\downarrow}b_{2g}$, $16^{\downarrow}a_g$, $3^{\downarrow}b_{3g}$, $2^{\downarrow}b_{2g}$, $15^{\downarrow}a_g$, $2^{\downarrow}b_{3g}$ MOs (Figure 16).

Similarly to $[Cu(acac)_2]$, the CDL UV−Vis spectrum (Figure 2) is characterized by two overlapping bands centered at 653 and 525 nm (1.90 and 2.35 eV, respectively) and, even if both CDL constituents contribute to them, the $\{Cu_2\}$ major role in the generation of the 525 nm feature has been recently established.[4] Moreover, the assignment of the $[Cu(acac)_2]$ spectrum indicates the contribution of 12, formally forbidden, d−d excitations (four for each *isolated* metal center) to the $\{Cu_3\}$ UV−Vis spectrum. According to that, the 12 spin−unrestricted TDDFT quartet−quartet $\{Cu_3\}$ lowest lying EEs are all characterized by very low f values ($2.0 \times 10^{-5} < f < 1.7 \times 10^{-4}$). Theoretical outcomes would then suggest assignment of the spectral feature centered at 653 nm (1.90 eV) to transitions having EEs at 1.64, 1.97, 1.97, 2.13 eV,[17] while those with EEs 2.33, 2.38, 2.38, and 2.43 eV should contribute to the CDL second feature at 2.35 eV.[18,19]

Despite the dispersive nature of the $\{G@Cu_3\}$ host−guest interaction, the presence of a fifth N-based ligand in the coordination sphere of three or two Cu^{2+} ions generate, in the energy region of the occupied frontier orbitals,[20] MOs having a Cu−N antibonding character (see Figure 19). Both this MO crowding around the $\{G@Cu_3\}$ HOMOs and the higher participation of Cu 3d AOs to MOs close to the $\{G@Cu_3\}$ HOMOs provide a rationale for the absorbance increase at 800

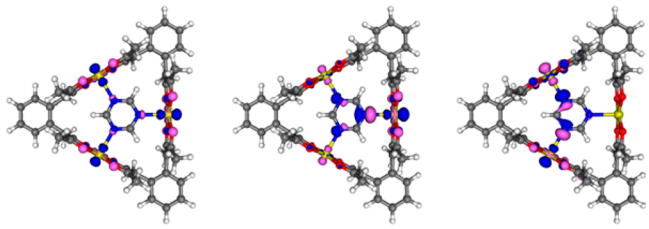

Figure 19. 3D contour plots of the $\{s\text{-}Tr@Cu_3\}$ $263^{\downarrow}a$ (left), $266^{\downarrow}a$ (middle), and $268^{\downarrow}a$ MOs. Pink (blue) surfaces correspond to the positive (negative) value of 0.05 (−0.05) $e^{1/2}$ Å$^{-3/2}$.

nm < λ < 1000 nm on passing from $[Cu(acac)_2]$/CDL to $\{G@Cu_3\}$ (much more evident for the adamantane-like guests than for the s-Tr and Pyr ones).

The wavelength region of the $\{G@Cu_3\}$ (G = HMT, PTA, PTAO) spectra extending from 490 to 1000 nm, besides the already mentioned absorbance increase for 800 nm < λ < 1000 nm, is dominated by an *intense* band centered at 620 nm (∼2.0 eV), very broad in $\{PTAO@Cu_3\}$, with a shoulder on its lower energy side both in $\{HMT@Cu_3\}$ and $\{PTA@Cu_3\}$. Once again the results of spin-unrestricted TDDFT quartet−quartet calculations[21−23] provide some useful information. The $\{G@Cu_3\}$ (G = HMT, PTA, PTAO) EEs spectrum up to 2.5 eV includes 12 excitations,[23] which group at ∼1.35, ∼1.80, and ∼2.30 eV and whose compositions indicate that (i) HOMOs → LUMOs transitions mainly contribute to EEs centered at ∼1.35 eV; (ii) guest based frontier MOs → LUMOs transitions contribute to EEs centered at ∼1.80 eV; (iii) Cu based Cu−O antibonding MOs → LUMOs transitions contribute to EEs centered at ∼2.30 eV. Accordingly, we tentatively assign the 800 nm < λ < 1000 nm energy region of the $\{G@Cu_3\}$ (G = HMT, PTA, PTAO) UV. Moreover, guest based frontier MOs → LUMOs transitions should be hidden, in the $\{HMT@Cu_3\}$ and $\{PTA@Cu_3\}$ spectra, under the shoulder at ∼730 nm (∼1.7 eV) and, in the $\{PTAO@Cu_3\}$ spectrum, under the lower energy side of the broad band centered at ∼650 nm (∼1.9 eV). Cu based Cu−O antibonding MOs → LUMOs transitions should instead contribute to the higher energy side of the band lying at 620 nm (2.0 eV) in the $\{HMT@Cu_3\}$ and $\{PTA@Cu_3\}$ spectra and at 650 nm (1.9 eV) in the $\{PTAO@Cu_3\}$ one.

The situation appears more complicated when $\{s\text{-}Tr@Cu_3\}$ and $\{Pyr@Cu_3\}$ are considered. In fact, their spectra are different not only from those of complexes with adamantane-like guest (see in Figure 2 the wavelength range 800 nm < λ < 1000 nm) but also between them. More specifically, the $\{s\text{-}Tr@Cu_3\}$ spectral pattern is characterized by two, strongly overlapping bands at 700 and 610 nm (∼1.80 and ∼2.10 eV), while the $\{Pyr@Cu_3\}$ one consists of a single broad band centered at 645 nm (∼1.90 eV) with an evident shoulder on its higher energy side (525 nm/∼2.4 eV). Once more, spin-unrestricted quartet−quartet TDDFT results shed light onto this complex matter. First of all, the $\{s\text{-}Tr@Cu_3\}$ and $\{Pyr@Cu_3\}$ EEs spectrum up to 2.5 eV includes only 9 for G = s-Tr and 10 for G = Pyr excitations rather than 12; furthermore, the lowest lying ones (three for G = s-Tr, two for G = Pyr) are at ∼1.70 eV.[23] Interestingly, the inspection of their compositions indicates that in both cases they do not imply $^{\downarrow}$HOMOs → $^{\downarrow}$LUMOs transitions,[21,24] rather excitations involving the occupied guest based MOs (Cu−N antibonding, Figure 19) hidden under peaks yz/z^2 ($\{s\text{-}Tr@Cu_3\}$) and yz ($\{Pyr@Cu_3\}$) in their spin ↓PDOS (see Figure 18) and corresponding

dx.doi.org/10.1021/ic500573e | *Inorg. Chem.* 2014, 53, 7276−7287

$^{\downarrow}$LUMOs. Before going on, it has to be remarked that the absence of EEs < 1.70 eV agrees very well with the already mentioned limited absorbance increase at 800 nm < λ < 1000 nm on passing from [Cu(acac)$_2$]/CDL to {G@Cu$_3$} (G = s-Tr, Pyr).

Even if the higher {s-Tr@Cu$_3$} and {Pyr@Cu$_3$} EEs may be grouped in two sets, at ∼1.90 and ∼2.40 eV in both complexes,[23] the situation is very different when looking at 2.40 < EEs < 2.90 eV: no excitation in the {s-Tr@Cu$_3$} EEs spectrum, four excitations, at 2.59, 2.65, 2.68, and 2.72 eV, in the {Pyr@Cu$_3$} one.[25] In both complexes, EEs centered at ∼1.90 imply HOMOs → LUMOs transitions,[22] while those at ∼2.40 eV correspond to genuine d−d excitations. Despite a slight overestimation, spin-unrestricted quartet−quartet TDDFT EEs allow us to propose the following assignment: the {s-Tr@Cu$_3$} band at 700 nm (∼1.80 eV) is associated with HOMOs → LUMOs transitions, while the feature at 610 nm (∼2.10 eV) is generated by d−d excitations.

Similarly to {s-Tr@Cu$_3$}, spin-unrestricted TDDFT results pertaining to {Pyr@Cu$_3$} prompt us to assign the low energy side of the single broad band characterizing its UV−Vis spectrum to excitations involving guest based frontier MOs (Cu−N antibonding) → LUMOs as well as HOMOs → LUMOs transitions, while the higher energy side of the same band should be generated by genuine d−d excitations. As far as the band shoulder at 525 nm (∼2.40 eV) is concerned, at least the 147$^{\downarrow}$a′ HOMO → 133$^{\downarrow}$a″ LUMO + 130$^{\downarrow}$a′ MO → 133$^{\downarrow}$a″ LUMO transition having EE = 2.59 eV should contribute to it.

CONCLUSIONS

The introduction of tailored guests allowed us to orchestrate the response of a CDL of copper coordination polygons. The guest is able to drive the selection of the CDL toward the target species, a metallo-supramolecular triangle, by forming a host−guest compound. Alternatively, the same guest is able to template the triangle self-assembly in a one-pot synthesis, by a VL approach. Selection is thermodynamically driven, according to a molecular recognition mechanism reminiscent of the enzymatic lock and key model. Host preorganization, in a triangular metallo-macrocycle, and host−guest complementarity play a crucial role in the molecular recognition process. Compounds have been fully characterized by UV−Vis absorption spectroscopy and structural studies through single crystal X-ray diffraction. All electron spin-unrestricted quartet−quartet TDDFT calculations including dispersive contributions allowed a thorough assignment of the host and host−guests spectral features, thus confirming the validity of the spin-unrestricted TDDFT approach to investigate spectral properties of open shell systems. The adopted theoretical approach was able to correctly model both structural and spectroscopic properties, whereas thermodynamic parameters along the investigated {G@Cu$_3$} series are less satisfactorily reproduced. The host−guest process has been fully studied considering a family of guest molecules characterized by different conformational flexibility, σ-donation strength and steric hindrance. Thermodynamic parameters for the host−guest process have been evaluated by variable temperature UV−Vis studies. The host−guest species can undergo guest exchange according to the following association constant scale: HMT > s-Tr > PTA ≈ PTAO > Pyr. Competition studies among different guests showed that the molecular recognition mechanism is highly selective for the {HMT@Cu$_3$} species. Remarkably, the selectivity among different guest pairs spans the 1−10^4 range, rising to 8.13 × 10^3 when one compares the two guests with the highest and lowest association constant. Hence, the molecular recognition based selection operates on a double level: guests act as CDL effectors selecting the triangular host from the dynamic systems of coordination polygons. At the same time, in the presence of a set of different competitive guests, the {Cu$_3$} triangular constituent of the CDL picks a specific guest according to a selectivity−affinity correlation.

EXPERIMENTAL SECTION

Reagents were purchased from Aldrich and used as received. The ligand 1,2-bis-(3-acetylacetone)benzene (*o*-LH$_2$),[11,26] PTA,[27] and PTAO[27] have been prepared as reported in the literature. The {Cu$_n$} (n = 2, 3) CDL has been prepared as previosly reported.[4]

Guest Induced Selection, General Procedure. A chloroform (1.0 mL) and methanol (0.4 mL) solution of G (0.05 mmol) was added to 5 mL of a {Cu$_n$} (n = 2, 3) chloroform solution (0.15 mmol of Cu^{2+} ions). The solution turned from olive green to blue-greenish. It was left under stirring for 1 h, and then the solvent was evaporated. Single crystals have been obtained after a few days, starting from different solvent mixtures as follows. Before elemental analysis single crystals were vacuum-dried overnight.

{HMT@Cu$_3$}. Single crystals (yield ≈ 95%) were obtained from chloroform/toluene, chloroform/*n*-hexane, chloroform/ethanol, and chloroform/benzene mixtures at room temperature. C 56.23%, N 4.92%, H 5.31% (exp.); C 56.51%, N 4.88%, H 5.27% (calc.).

{s-Tr@Cu$_3$}. Single crystals (yield ≈ 95%) were obtained from chloroform/*n*-hexane, chloroform/cyclohexane, and chloroform/decane mixtures at −18 °C. C 56.35%, N 3.74%, H 4.63% (exp.); C 56.27%, N 3.86%, H 4.72% (calc.).

{PTA@Cu$_3$}. Single crystals (yield ≈ 80%) were obtained from a chloroform/*n*-hexane mixture at 4 °C. C 59.51%, N 2.65%, H 5.73% (exp.); C 59.66%, N 2.58%, H 5.56% (calc.).

{PTAO@Cu$_3$}. Single crystals (yield ≈ 95%) were obtained from chloroform/toluene and chloroform/acetonitrile mixtures at room temperature. C 58.73%, N 2.48%, H 5.33% (exp.); C 58.80%, N 2.54%, H 5.48% (calc.).

{Pyr@Cu$_3$}. Single crystals (yield ≈ 70%) were obtained from chloroform/decane at −18 °C. C 57.57%, N 2.49%, H 4.89% (exp.); C 57.43%, N 2.58%, H 4.82% (calc.).

G = Me−Tr. No reaction was observed with this molecule. The resulting solution was left under stirring for 2 days. UV−Vis absorption spectra showed the formation of the dimer−trimer CDL indicating that Me−Tr does not react with the {Cu$_n$} (n = 2, 3) system.

Templated Self-Assembly, General Procedure. CuSO$_4$·5(H$_2$O) (0.35 mmol) was dissolved in 3 mL of water and converted to [Cu(NH$_3$)$_4$]$^{2+}$ by addition of a NH$_3$ solution (28%) in excess (1−2 mL). Alternatively, a copper acetate water solution can be used instead of the [Cu(NH$_3$)$_4$]$^{2+}$ solution. This solution was added to a chloroform (5 mL) and methanol (1 mL) solution of *o*-LH$_2$ (0.3 mmol) and G (0.1 mmol). The biphasic system was stirred for 3 h. The two phases were separated, and the organic one was evaporated under reduced pressure. Single crystals were obtained after a few days, starting from different solvent mixtures as reported above.

No host−guest species could be obtained using Me−Tr as guest. The reaction in the presence of this guest led to the formation of the {Cu$_n$} (n = 2, 3) CDL.

Competition Reaction via Guest Induced Selection. A chloroform (5 mL) and methanol (1 mL) solution of the five guests (0.10 mmol of HMT, 0.10 mmol of s-Tr, 0.10 mmol of PTA, 0.10 mmol of PTAO and 0.10 mmol of Pyr) was added to 5 mL of a {Cu$_n$} (n = 2, 3) chloroform solution (0.30 mmol of Cu^{2+} ions). The solution turned from olive green to blue-greenish. It was left under stirring for 2 h. Single crystals of {HMT@ Cu$_3$}, in quantitative yield, were obtained from chloroform/*n*-hexane or chloroform/toluene solutions.

Competition Reaction via Guest Templated Self-Assembly. CuSO$_4$·5H$_2$O (0.63 mmol) was dissolved in 5 mL of water and converted to [Cu(NH$_3$)$_4$]$^{2+}$ by addition of a NH$_3$ solution (28%) in

dx.doi.org/10.1021/ic500573e | Inorg. Chem. 2014, 53, 7276−7287

excess (1−2 mL). This solution was added to a chloroform (10 mL) and methanol (1 mL) solution of *o*-LH_2 (0.59 mmol), HMT (0.40 mmol), s-Tr (0.39 mmol), and PTA (0.40 mmol), PTAO (0.40 mmol) and Pyr (0.40 mmol).The biphasic system was stirred for 2 h. The two phases were separated, and the organic one was evaporated and dried under a vacuum overnight. Single crystals of {HMT@ Cu_3}, in quantitative yield, were obtained from chloroform/*n*-hexane or chloroform/toluene solutions.

Equilibrium Constant Determination, General Procedure. Absorption spectra were recorded on a CARY 4000 double beam spectrophotometer equipped with a Peltier thermostat. In a quartz-Suprasil cuvette (equipped with a screw cap), to 3.0 mL of a chloroform stock solution of {Cu_n} (n = 2, 3) CDL, a chloroform stock solution of the guest was added in different aliquots. Absorption spectra were recorded at different temperatures after each addition according to Tables S20−S24 in Supporting Information. Spectra are shown in Figures S8−S28. Titration data were computed using Hyperquad software[30] according to the model described in Supporting Information.

X-ray Crystallography. Single crystals were fastened on the top of a Lindemann glass capillary or mounted using Paratone-N oil and centered on the head of a four-circle kappa goniometer Oxford Diffraction Gemini E diffractometer, equipped with a 2K × 2K EOS CCD area detector and sealed-tube Enhance (Mo) and (Cu) X-ray sources. Mo Kα (λ = 0.71070 Å) radiation was used for all data collections. Data were collected at room temperature by means of the ω-scans technique using graphite-monochromated radiation, in a 1024 × 1024 pixel mode, using 2 × 2 pixel binning. The diffraction intensities were corrected for Lorentz and polarization effects and were also optimized with respect to absorption. Empirical multi-scan absorption corrections using equivalent reflections were performed with the scaling algorithm *SCALE3 ABSPACK*. Data collection, data reduction, and finalization were carried out through the CrysAlisPro software. Structures were solved by means of direct methods using SHELXS[28] or charge flipping with OLEX2[29] and refined by full-matrix least-squares methods based on F_0^2 with SHELXL[28] in the framework of OLEX2[29] software. In the last cycles of refinement, ordered non-hydrogen atoms were refined anisotropically, whereas disordered partial occupancy non-hydrogen atoms were refined isotropically. Hydrogen atoms connected to carbon atoms were included in idealized positions, and a riding model was used for their refinement. The crystal parameters and information pertaining to the data collection, solution, and refinement are detailed in Supporting Information along with bond distances and angles (Tables S1−S19). Selected values are provided in the figure captions. CCDC 971592−971596, 971598, and 971599 contain the supplementary crystallographic data for this paper. These data can be obtained free of charge from Cambridge Crystallographic Data Center via www.ccdc.cam.ac.uk/data_request/cif.

Computational Details. Density functional theory (DFT) calculations were carried out by using the ADF 2013 package.[31] Both the electronic and structural properties of the investigated molecules were obtained by using the hybrid Becke3−Lee−Yang−Parr (B3LYP) exchange correlation functional, i.e., by combining a standard generalized gradient (VWN5) with a part (20%) of Hartree−Fock exchange.[32] All electrons DZP basis sets were used for typical elements, while an all electrons TZP basis set was adopted for Cu atoms. Numerical experiments pertaining to {Cu_3} and {G@Cu_3} were run by including spin−polarization effects and by assuming the presence of three unpaired electrons. Optimized geometrical parameters were obtained without any symmetry constraint for {Cu_3} and {G@Cu_3} (G = s-Tr and Pyr), while a C_s symmetry was adopted for {G@Cu_3} (G = HMT, PTA, PTAO).

The Cu_3−G binding energy (BE) was analyzed by using the Ziegler's extended transition-state method[10]

$$BE = \Delta E_{elstat} + \Delta E_{Pauli} + \Delta E_{int} + \Delta E_{prep}$$

where ΔE_{elstat} is the pure electrostatic interaction, ΔE_{Pauli} corresponds to the destabilizing two-orbital, four-electron interaction between the occupied orbitals of the two interacting fragments (ΔE_{elstat} + ΔE_{Pauli} = ΔE_{steric}), ΔE_{int} derives from the stabilizing interaction between occupied and empty orbitals of the fragments, and the last term, ΔE_{prep}, is the energy required to relax the structure of the free fragments to the geometry of the final system. BE values were further corrected by taking into account dispersive contributions, which were included by adding a dispersion correction[33] to the total bonding energy and to the gradients. Information about the localization and the bonding/antibonding character of selected molecular orbitals (MOs) over a broad range of energy was obtained by referring to the density of states (DOS), partial DOS (PDOS), and crystal orbital overlap population (COOP).[34] Corresponding curves were computed by weighting one-electron energy levels by their basis orbital percentage and by applying a 0.25 eV Lorentzian broadening. These plots, based on the Mulliken's prescription for partitioning the overlap density,[35] allow an easy inspection of the atomic composition of MOs over a broad range of energy. We are perfectly aware that the Mulliken's prescription for partitioning the overlap density, even though uniquely defined, is rather arbitrary; nevertheless, it yields at least a qualitative idea of the electron localization. Finally, 3D contour plots were obtained to get information about the localization and the bonding/antibonding character of selected MOs.

■ ASSOCIATED CONTENT

Ⓢ Supporting Information

X-ray details pertaining to the data collection, solution, and refinement along with bond distances and angles. Spectroscopic UV−Vis studies: variable temperature titrations, data analysis and van't Hoff plots. Cartesian coordinates of optimized structures. This material is available free of charge via the Internet at http://pubs.acs.org.

■ AUTHOR INFORMATION

Corresponding Author

*E-mail: marzio.rancan@unipd.it.

Notes

The authors declare no competing financial interest.

■ ACKNOWLEDGMENTS

This work was supported by Italian MIUR through FIRB RBAP114AMK "RINAME". The Community of Computational Chemistry of the University of Padova (C_3P) at the Department of Chemical Sciences is acknowledged for support of the computer facilities. J.T. thanks the CaRiPaRo Foundation for a Ph.D. scholarship. M.R. thanks the University of Padova for a "Senior Research" fellowship and for a "Young Scholar" grant.

■ REFERENCES

(1) Lehn, J.-M. *Angew. Chem., Int. Ed.* **2013**, *52*, 2836−2850.
(2) For recent reviews see: (a) Chakrabarty, R.; Mukherjee, P. S.; Stang, P. J. *Chem. Rev.* **2011**, *111*, 6810−6918. (b) Ward, M. D.; Raithby, P. R. *Chem. Soc. Rev.* **2013**, *42*, 1619−1636. (c) Smulders, M. M. J.; Riddell, I. A.; Browne, C.; Nitschke, J. R. *Chem. Soc. Rev.* **2013**, *42*, 1728−1754.
(3) (a) Fujita, M.; Sasaki, O.; Mitsuhashi, T.; Fujita, T.; Yazaki, J.; Yamaguchi, K.; Ogura, K. *Chem. Commun.* **1996**, 1535−1536. (b) Yamamoto, T.; Arif, A. M.; Stang, P. J. *J. Am. Chem. Soc.* **2003**, *125*, 12309−12317. (c) Weilandt, T.; Troff, R. W.; Saxell, H.; Rissanen, K.; Schalley, C. A. *Inorg. Chem.* **2008**, *47*, 7588−7598. (d) Cotton, F. A.; Murillo, C. A.; Yu, R. *Dalton Trans.* **2006**, *32*, 3900−3905. (e) Ferrer, M.; Pedrosa, A.; Rodrìguez, L.; Rossell, O.; Vilaseca, M. *Inorg. Chem.* **2010**, *49*, 9438−9449. (f) Ghosh, S.; Mukherjee, P. S. *Inorg. Chem.* **2009**, *48*, 2605−2613. (g) Schweiger, M.; Seidel, S. R.; Arif, A. M.; Stang, P. J. *Inorg. Chem.* **2002**, *41*, 2556−2559. (h) Uehara, K.; Kasai, K.; Mizuno, N. *Inorg. Chem.* **2010**, *49*, 2008−2015. (i) Kraus, T.; Buděšonský, M.; Cvačka, J.; Sauvage, J.-P.

Angew. Chem., Int. Ed. **2006**, *45*, 258−261. (j) Suzuki, K.; Kawano, M.; Fujita, M. *Angew. Chem., Int. Ed.* **2007**, *46*, 2819−2822. (k) W. Baxter, P. N.; Khoury, R. G.; Lehn, J.-M.; Baum, G.; Fenske, D. *Chem.—Eur. J.* **2000**, *6*, 4140−4148. (l) Meng, W.; Ronson, T. K.; Clegg, J. K.; Nitschke, J. R. *Angew. Chem., Int. Ed.* **2013**, *52*, 1017−1021. (m) Hasenknopf, B.; Lehn, J.-M.; Boumediene, N.; Dupont-Gervais, A.; Van Dorsselaer, A.; Kneisel, B.; Fenske, D. *J. Am. Chem. Soc.* **1997**, *119*, 10956−10962. (n) Scherer, M.; Caulder, D. L.; Johnson, D. W.; Raymond, K. N. *Angew. Chem., Int. Ed.* **1999**, *38*, 1587−1592. (o) Kubota, Y.; Sakamoto, S.; Yamaguchi, K.; Fujita, M. *Proc. Natl. Acad. Sci. U. S. A.* **2002**, *99*, 4854−4856. (p) Campos-Fernández, C. S.; Schottel, B. L.; Chifotides, H. T.; Bera, J. K.; Bacsa, J.; Koomen, J. M.; Russell, D. H.; Dunbar, K. R. *J. Am. Chem. Soc.* **2005**, *127*, 12909−12923. (q) Riddell, I. A.; Smulders, M. M. J.; Clegg, J. K.; Hristova, Y. R.; Breiner, B.; Thoburn, J. D.; Nitschke, J. R. *Nat. Chem.* **2012**, *4*, 751−756. (r) Riddell, I. A.; Hristova, Y. R.; Clegg, J. K.; Wood, C. S.; Breiner, B.; Nitschke, J. R. *J. Am. Chem. Soc.* **2013**, *135*, 2723−2733. (s) Bar, A. K.; Raghothama, S.; Moon, D.; Mukherjee, P. S. *Chem.—Eur. J.* **2012**, *18*, 3199−3209.

(4) Rancan, M.; Tessarolo, J.; Zanonato, P. L.; Seraglia, R.; Quici, S.; Armelao, L. *Dalton Trans.* **2013**, *42*, 7534−7538.

(5) Rancan, M.; Dolmella, A.; Seraglia, R.; Orlandi, S.; Quici, S.; Armelao, L. *Chem. Commun.* **2012**, *48*, 3115−3117.

(6) (a) Lehn, J.-M. *Top. Curr. Chem.* **2012**, *322*, 1−32. (b) Lehn, J.-M. *Chem. Soc. Rev.* **2007**, *36*, 151−160.

(7) (a) Lehn, J.-M. *Proc. Natl. Acad. Sci. U.S.A.* **1997**, *94*, 2106−2110. (b) Lehn, J.-M. *Chem.—Eur. J.* **1999**, *5*, 2455−2463.

(8) Steed, J. W.; Atwood, J. L. *Supramolecular Chemistry*, 2nd ed; Wiley: New York, 2009.

(9) Schneider, H.−J.; Yatsimirsky, A. K. *Chem. Soc. Rev.* **2008**, *37*, 263−277.

(10) Ziegler, T.; Rauk, A. *Theor. Chim. Acta* **1977**, *46*, 1−10.

(11) Rancan, M.; Dolmella, A.; Seraglia, R.; Orlandi, S.; Quici, S.; Sorace, L.; Gatteschi, D.; Armelao, L. *Inorg. Chem.* **2012**, *51*, 5409−5416.

(12) de Almeida, K. J.; Cesar, A.; Rinkevicius, Z.; Vahtras, O.; Ågren, H. *Chem. Phys. Lett.* **2010**, *492*, 14−18.

(13) $[Cu(acac)_2]$ Cartesian coordinates optimized by including dispersive contributions are reported in Table S41.

(14) (a) Wang, F.; Ziegler, T. *Mol. Phys.* **2004**, *102*, 2585−2595. (b) In the recent past, the same approach has been successfully applied by Nardi et al. to investigate near edge X-ray absorption fine structure spectra of CuPc.[14c] (c) Nardi, M. V.; Detto, F.; Aversa, L.; Verucchi, R.; Salviati, G.; Iannotta, S.; Casarin, M. *Phys. Chem. Chem. Phys.* **2013**, *15*, 12864−12881.

(15) Initial/final state contributions smaller than 10% are not reported.

(16) The neglecting of any vibronic coupling implies that the oscillator strength *f* of the four $[Cu(acac)_2]$ lowest lying excitations is zero.

(17) The four lowest lying transitions have the following compositions: (1.64 eV; $256^{\downarrow}a \rightarrow 259^{\downarrow}a$ (30%) + $258^{\downarrow}a \rightarrow 259^{\downarrow}a$ (17%) + $255^{\downarrow}a \rightarrow 259^{\downarrow}a$ (16%) + $228^{\downarrow}a \rightarrow 259^{\downarrow}a$ (12%) + $230^{\downarrow}a \rightarrow 259^{\downarrow}a$ (11%)); (1.97 eV; $258^{\downarrow}a \rightarrow 260^{\downarrow}a$ (26%) + $257^{\downarrow}a \rightarrow 260^{\downarrow}a$ (15%) + $257^{\downarrow}a \rightarrow 261^{\downarrow}a$ (12%)); (1.97 eV; $258^{\downarrow}a \rightarrow 261^{\downarrow}a$ (26%)); (2.13 eV; $243^{\downarrow}a \rightarrow 259^{\downarrow}a$ (69%)).

(18) Fifth to eighth (2.33, 2.38, 2.38, 2.43 eV) and nineth to 12th (2.51, 2.66, 2.66, 2.67 eV) EEs imply transitions from Cu based MOs (Cu−O antibonding in nature) to $\{Cu_3\}$ LUMOs.

(19) The EE at 2.13 eV corresponds to the EE of the first genuine d−d transition; both the $243^{\downarrow}a$ and the $259^{\downarrow}a$ MOs are in fact strongly localized (31 and 58%, respectively) on the same Cu^{2+} ion. The $243^{\downarrow}a$ level generates the *yz* peak at −7.90 eV in the $\{Cu_3\}$ 3d spin ↓ PDOS (Figure 18).

(20) Miessler, G. L.; Fischer, P. J.; Tarr, D. A. *Inorganic Chemistry*, 5th ed.; Pearson: London, 2013.

(21) $\{G@Cu_3\}$ ↓HOMOs (↓LUMOs) correspond to the following MOs: G = HMT, $137^{\downarrow}a''$ + $138^{\downarrow}a''$ + $158^{\downarrow}a'$ at −5.91, −5.88, −5.87 eV, respectively ($159^{\downarrow}a'$ + $139^{\downarrow}a''$ + $140^{\downarrow}a''$ at −2.52, −2.51, −2.46 eV, respectively); G = PTA, $138^{\downarrow}a''$ + $139^{\downarrow}a''$ + 161a′ at −5.90, −5.78, −5.77 eV, respectively ($162^{\downarrow}a'$ + $140^{\downarrow}a''$ + $141^{\downarrow}a''$ at −2.56, −2.55, −2.47 eV, respectively); G = PTAO, $139^{\downarrow}a''$ + $140^{\downarrow}a''$ + 164a′ at −6.01, −5.87, −5.86 eV, respectively ($165^{\downarrow}a'$ + $141^{\downarrow}a''$ + $142^{\downarrow}a''$ at −2.66, −2.66, −2.58 eV, respectively); G = s−Tr, $97^{\downarrow}a_1$ + $98^{\downarrow}a_1$ + $88^{\downarrow}b_2$ at −6.35, −6.12, −5.98 eV, respectively ($45^{\downarrow}a_2$ + $50^{\downarrow}b_1$ + $46^{\downarrow}a_2$ at −2.51, −2.50, −2.49 eV, respectively); G = Pyr, $147^{\downarrow}a'$ + $131^{\downarrow}a''$ + 132a″ at −5.93, −5.91, −5.78 eV, respectively ($133^{\downarrow}a''$ + $148^{\downarrow}a'$ + $134^{\downarrow}a''$ at −2.66, −2.32, −2.31 eV, respectively).

(22) To overcome severe convergence problems, TDDFT calculations pertaining to $\{s\text{-}Tr@Cu_3\}$ and $\{Pyr@Cu_3\}$ have been run by assuming C_{2v} and C_s optimized geometries, respectively. The ΔBE between C_{2v} and C_1 (C_s and C_1) optimized structures amounts to 0.00 (1.76) kJ/mol.

(23) $\{G@Cu_3\}$ EEs < 2.50 eV have the following symmetries and values: G = HMT, a′ at 1.35, 1.81, 1.85, 2.28, 2.32 eV; a″ at 1.35, 1.36, 1.81, 2.28, 2.32, 2.32, 2.33 eV; G = PTA, a′ at 1.37, 1.79, 1.85, 2.26, 2.32 eV; a″ at 1.35, 1.36, 1.79, 2.26, 2.32, 2.32, 2.34 eV; G = PTAO, a′ at 1.44, 1.81, 1.86, 2.31, 2.34 eV; a″ at 1.42, 1.44, 1.81, 2.31, 2.34, 2.35, 2.37 eV; G = s-Tr, a_2 at 1.72, 1.74, 1.91, 2.38, 2.39 eV; b_1 at 1.72, 1.91, 1.92, 2.39 eV; G = Pyr, a′ at 1.71, 1.89, 1.93, 2.39, 240 eV; a″ at 1.70, 1.89, 2.34, 2.39, 2.40 eV.

(24) The three $\{s\text{-}Tr@Cu_3\}$ lowest lying excitations have the following compositions: (1.72 eV; $85^{\downarrow}b_2 \rightarrow 50^{\downarrow}b_1$ (30%) + $94^{\downarrow}a_1 \rightarrow 46^{\downarrow}a_2$ (16%)); (1.74 eV; $95^{\downarrow}a_1 \rightarrow 45^{\downarrow}a_2$ (34%) + $94^{\downarrow}a_1 \rightarrow 45^{\downarrow}a_2$ (18%) + $97^{\downarrow}a_1 \rightarrow 45^{\downarrow}a_2$ (12%)); (1.72 eV; $85^{\downarrow}b_2 \rightarrow 46^{\downarrow}a_2$ (27%) + $94^{\downarrow}a_1 \rightarrow 50^{\downarrow}b_1$ (17%) + $95^{\downarrow}a_1 \rightarrow 50^{\downarrow}b_1$ (11%)). The two $\{Pyr@Cu_3\}$ lowest lying excitations have the following compositions: (1.71 eV; $141^{\downarrow}a' \rightarrow 148^{\downarrow}a'$ (28%) + $128^{\downarrow}a'' \rightarrow 134^{\downarrow}a''$ (20%) + $131^{\downarrow}a'' \rightarrow 134^{\downarrow}a''$ (12%)); (1.70 eV: $141^{\downarrow}a' \rightarrow 134^{\downarrow}a''$ (28%) + $128^{\downarrow}a'' \rightarrow 148^{\downarrow}a'$ (20%) + $131^{\downarrow}a'' \rightarrow 148^{\downarrow}a'$ (12%)).

(25) The three $\{s\text{-}Tr@Cu_3\}$ lowest lying excitations have the following compositions: (1.72 eV; $85^{\downarrow}b_2 \rightarrow 50^{\downarrow}b_1$ (30%) + $94^{\downarrow}a_1 \rightarrow 46^{\downarrow}a_2$ (16%)); (1.74 eV; $95^{\downarrow}a_1 \rightarrow 45^{\downarrow}a_2$ (34%) + $94^{\downarrow}a_1 \rightarrow 45^{\downarrow}a_2$ (18%) + $97^{\downarrow}a_1 \rightarrow 45^{\downarrow}a_2$ (12%)); (1.72 eV; $85^{\downarrow}b_2 \rightarrow 46^{\downarrow}a_2$ (27%) + $94^{\downarrow}a_1 \rightarrow 50^{\downarrow}b_1$ (17%) + $95^{\downarrow}a_1 \rightarrow 50^{\downarrow}b_1$ (11%)). The two $\{Pyr@Cu_3\}$ lowest lying excitations have the following compositions: (1.71 eV; $141^{\downarrow}a' \rightarrow 148^{\downarrow}a'$ (28%) + $128^{\downarrow}a'' \rightarrow 134^{\downarrow}a''$ (20%) + $131^{\downarrow}a'' \rightarrow 134^{\downarrow}a''$ (12%)); (1.70 eV: $141^{\downarrow}a' \rightarrow 134^{\downarrow}a''$ (28%) + $128^{\downarrow}a'' \rightarrow 148^{\downarrow}a'$ (20%) + $131^{\downarrow}a'' \rightarrow 148^{\downarrow}a'$ (12%)).

(26) Ramirez, F.; Bhatia, S. B.; Patwardhan, A. V.; Smith, C. *J. Org. Chem.* **1967**, *32*, 3547−3553.

(27) Daigle, D. J.; Pepperman, A. B., Jr.; Vail, S. L. *J. Heterocyclic Chem.* **1974**, *11*, 407−408.

(28) Sheldrick, G. M. *Acta Crystallogr.* **2008**, *A64*, 112−122.

(29) Dolomanov, O. V.; Bourhis, L. J.; Gildea, R. J.; Howard, J. A. K.; Puschmann, H. *J. Appl. Crystallogr.* **2009**, *42*, 339−341.

(30) Gans, P.; Sabatini, A.; Vacca, A. *Talanta* **1996**, *43*, 1739−1753.

(31) Amsterdam Density Functional (ADF) version 2013.01. http://www.scm.com.

(32) Stephens, P. J.; Devlin, F. J.; Chabalowski, C. F.; Frisch, M. J. *J. Phys. Chem.* **1994**, *98*, 11623−11627.

(33) Grimme, S.; Ehrlich, S.; Goerigk, L. *J. Comput. Chem.* **2011**, *32*, 1456−1465.

(34) Hoffmann, R. *Solids and Surfaces: A Chemist's View of Bonding in Extended Structures*; VCH: New York, 1988.

(35) Mulliken, R. S. *J. Chem. Phys.* **1955**, *23*, 1833−1840.